CHAPTER 2: PRE-BLOUBERG, WATERBERG AND SOUTPANSBERG ROCKS.

The lithologies which pre-date the Blouberg, Waterberg and Soutpansberg Group rocks generally outcrop at relatively low altitudes amongst the lower slopes of Blouberg mountain, and more rarely outcrop on the flat-lying terrain to the north and south of Blouberg (Appendix 1). At areas around 23°06.20'S; 29°00.50'E, these rocks underlie areas of relatively high altitude (locally up to 1500m), immediately to the north of the southern strand of the Melinda Fault. Rarely, outcrops of these rocks can also be found in the low-lying area to the east of the Makgabeng plateau, though these lie outside the study area. Generally these rocks consist of a well foliated quartzo-feldspathic gneiss (Fig. 2.1) which can be considered to be a basement complex to the overlying non-metamorphosed or low-grade strata in the field area.

A photomicrograph of a typical gneiss in the field area is shown in Figure 2.2, and shows that minor biotite is also present in addition to quartz and feldspar, which is commonly developed along foliation planes. Amphibolite lenses are also well developed in many areas, with the long axis of the lenses orientated parallel to the strike of the foliation plane (Figure. 2.1). The length of the lenses varies from 10cm to several metres, and can be 2 to 3m wide. A thin section from an amphibolite lens is shown in Figure 2.3, which shows intergrown amphibole, feldspar and quartz. Generally quartz is rare in these amphibolitic rocks.

The feldspar- and amphibolite-rich basement rocks generally weather easily to produce a thick soil, and as a result outcrops of these rocks are rare in the study area, and measurements relating to their structural geology can only rarely be recorded. Outcrops are generally limited to stream beds where weathered material is commonly eroded resulting in fresh surfaces being exposed.

The orientations of foliation planes recorded in basement gneiss throughout the field area are shown in Figure 2.4, which indicates that the foliation planes generally dip vertically to sub-vertically, and generally strike W.S.W. to E.N.E. In many locations (e.g. 23°05.12'S; 29°01.93'E) the sense of shearing within the gneiss can be determined. W.S.W.-E.N.E. -trending boudins formed between the foliated layers (Figure 2.5) indicate shearing in this orientation, and vertically plunging asymmetric 'S' folds suggest sinistral strike-slip movement along an 080° striking, vertically dipping shear zone (Figures 2.6 and 2.7) The orientation of foliation planes in 'S'-shaped folded gneiss are shown in Figure 2.8., which indicates their vertical fold axis. A sinistral sense of movement within the gneiss can also be gained from stair-stepping porphyroclasts (as defined by Passchier and Trouw, 1998) (Figure 2.1). Figure 2.9 shows evidence for multiple deformation: An asymmetric 'S' fold (indicating sinistral movement along an 070°-striking shear zone) is displaced 30 cm by a 080° striking dextral ductile shear zone. Generally, the orientation of foliation planes recorded in the outcrops of gneiss suggests that the foliation is fairly consistent throughout the study area. Due to the paucity of outcrops of basement lithologies, it was not possible to identify any regional variation or discrete domains of specific foliation orientation within the gneiss.

Locally, however, the orientation of foliation planes differs due to folding (Figure 2.6), partial melting, injection of melt or interference folding (Figure 2.10) or due to super-imposed multiple generations of ductile deformation. A large-scale map showing the strike of sub-vertically and vertically dipping foliation planes in basement gneiss at 23°05.21'S, 28°47.53'E, in a stream bed 1km west of My Darling (23°05.21'S; 28°47.53'E) is shown in Figure 2.11. This map, which is divided into a grid of $5m^2$, shows that foliation orientation also varies over a larger scale. Figure 2.11 shows that at least two orientations of foliations are developed in the My Darling area (D_1 and D_2), with evidence locally for the presence of a third (D_3). An earlier sinistral shear zone (D_1) strikes approximately N.E.-S.W., and is subsequently deformed by a secondary cross-cutting shear zone (D_3) which strikes approximately east-west. Drag folding of primary foliation (S_1) along the edges of secondary shear zones (e.g. grid square F/12 in Figure 2.11) can be interpreted to have formed during dextral shearing along the secondary shear

zones. Secondary foliation (S_2) is best developed within a c. 5m wide shear zone in grid squares F/13 and E/14 (Figure 2.11). Evidence can also be seen for locally developed N.W.-S.E.-trending tertiary shear zones (D_3) , which cross-cut secondary foliation planes in grid squares F/6 and F/7. Generally tertiary shear zones also appear to have a dextral displacement, and are sub-parallel to the secondary shear zones. Shear zones cutting primary foliation in grid squares B/9 and B/10 (Figure 2.12) may be either secondary or tertiary. Rose histograms of the strike of foliations in primary and secondary shear zones are provided in Figure 2.13, and show that primary foliation planes dominantly strike N.E. to S.W., whilst secondary foliation planes dominantly strike east-west.

In contrast to the foliated gneiss described above, where distinct banding is visible between the segregated mineral layers, many of the outcrops which have been previously mapped as basement gneiss (e.g. Jansen, 1976; Geological Survey, 1985) differ locally. Rocks which outcrop against along the southern side of Blouberg mountain, and are adjacent to the inferred position of the southern strand of the Melinda Fault Zone (Appendix 1) differ from the common crystalline quartzo-feldspathic and amphibolitic gneiss in the field area. These rocks are more granular, and generally friable when weathered (Figure 2.14), and lack amphibolite-rich layers which are characteristics of the gneiss elsewhere in the field area. Locally, the rocks closely resemble a crush microbreccia (using the classification scheme of fault rocks of Roering *et al.*, 1989). They are, however, generally intruded by narrow (3-4mm) quartz-filled veins (Figure 2.15). Though this rock proved too friable for thin section analysis, such veins may also be locally found intruding the foliated basement gneiss adjacent to the edge of the southern strand of the Melinda Fault, such as that shown in thin section in Figure 2.16. Figure 2.16 shows that the vein quartz is relatively undeformed compared to the neighbouring crystals of quartz and feldspar within the gneiss. The orientation of the pervasive quartz veins in the microbreccias and gneiss are shown in Figure 2.17, which have a comparable orientation to the foliation of the gneiss not affected by quartz veining shown in Figure 2.4. The resemblance of the geometry of veins intrusive within the microbreccia to the foliation in the gneiss may have led earlier workers (e.g. Jansen, 1976; Geological Survey, 1985) to have mapped the veined microbreccia as a foliated gneiss. However, the

differences between these two lithologies suggest that a different mechanism was responsible for the veined microbreccia to that of the banded gneiss. The mechanism responsible for such microbreccia is likely to have been faulting under brittle conditions, in comparison to the highly ductile conditions under which banded, foliated gneiss is likely to have formed. As such, many of the rocks previously mapped as basement gneiss should rather be considered as younger faults and will be considered further in Chapter 7 (map relationships and structural geology).

The contact between the basement gneiss or crush breccia of the southern strand of the Melinda Fault and the overlying strata of the Blouberg Formation is locally marked by the presence of a dark red or brown hydrothermally altered rock containing ubiquitous jasper and quartz veins (Figure 2.18). These hydrothermally altered zones may locally reach a thickness of around 5m.

In addition to the crush-breccia described above, other examples of subsequent brittle structures affecting basement rocks were only rarely recorded. Locally slickensides and evidence for thrust faulting can be found within basement rocks, and these are described more fully in Section 7.1. The general paucity of evidence for brittle reactivation in basement rocks may be explained by the fact that the constituent minerals of basement rocks can be readily weathered (e.g. feldspar and amphibolites), and by the friability of brittle structures, which leads to increased rates of erosion. Brittle structures in basement rocks are therefore likely to form negative relief, and so it is unlikely that these structures will crop out and be recorded.

Figure 2.1: Quartzo-feldspathic banded gneiss with dark amphibolite lenses, exhibiting vertically-dipping, 080°-striking foliation. Sub-euhedral feldspar porphyroclasts show stair-stepping, and suggest sinistral movement along the foliation plane. Compass is 6cm wide, and points north. Recorded at 23°05.40'S; 29°01.53'E.

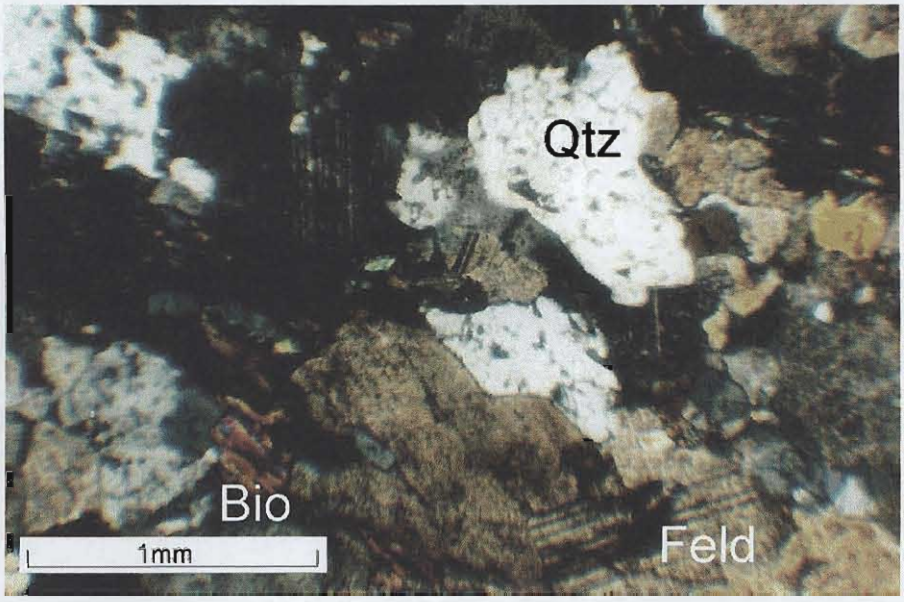

Figure 2.2: Photomicrograph of a thin section of basement gneiss. Constituent minerals are quartz, feldspar and minor biotite.

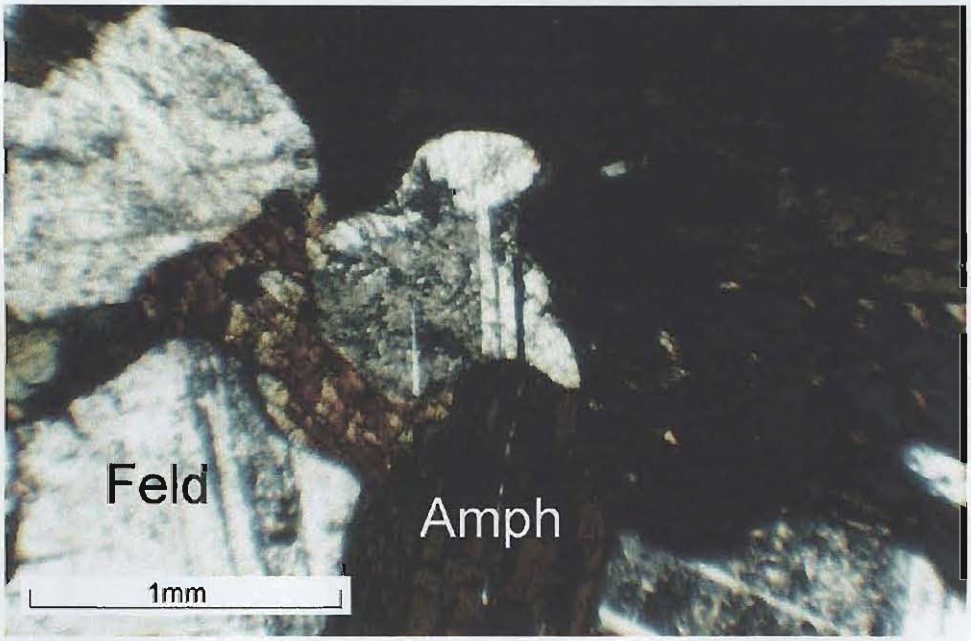

Figure 2.3: Photomicrograph of a thin section from an amphibolite lens in banded gneiss. Constituent minerals are amphibole and feldspar.

Figure 2.5: Banded gneiss at 23°05.12'S: 29°01.53'E, which shows a 080°-striking foliation, exhibiting boudinage of competent quartzo-feldspathic layers within the less competent amphibolite-rich layers. A 4cm-wide pegmatite vein cuts the outcrop. Compass is 6cm wide, and is orientated towards the north.

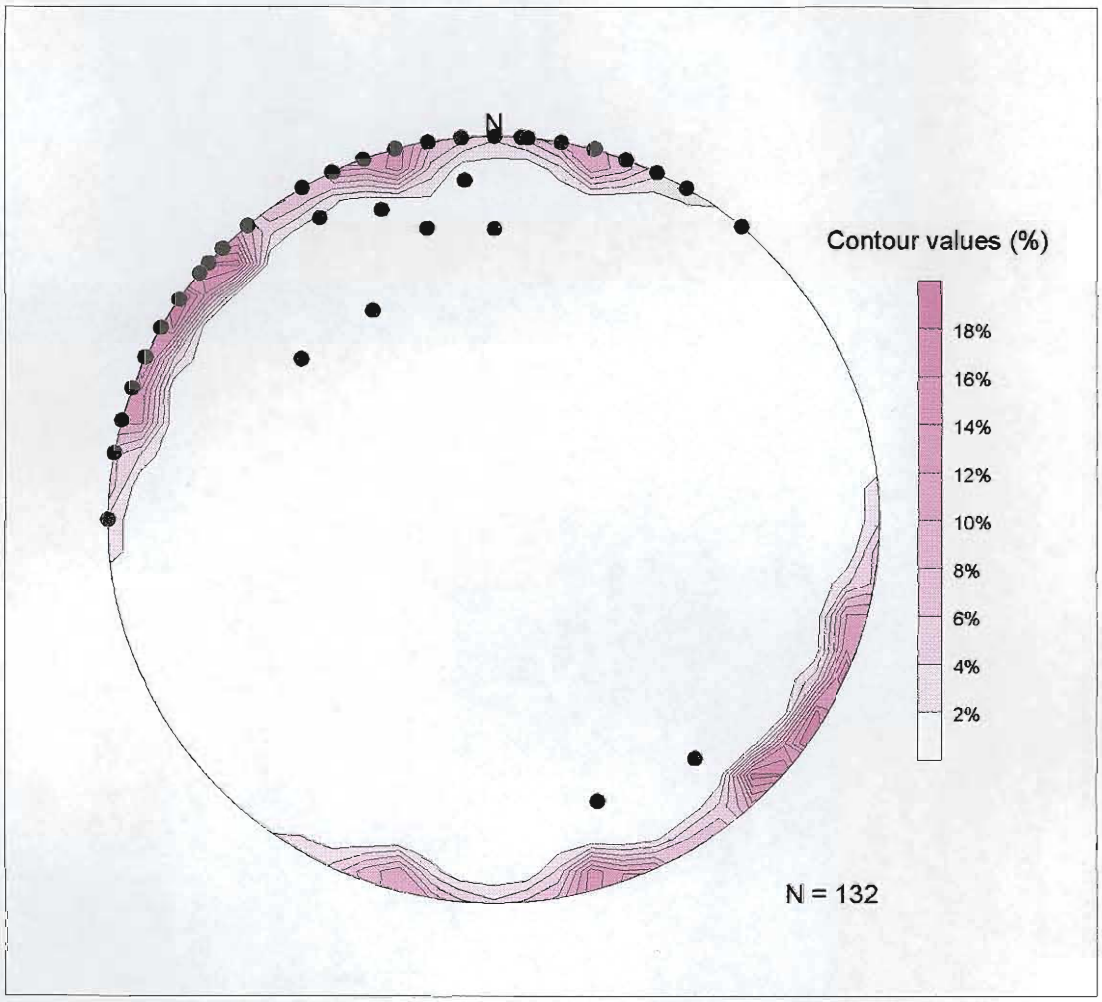

Figure 2.4: Stereographic projection showing the poles of generally vertically-dipping foliation planes recorded in basement gneiss.

Figure 2.6: Local variation in the orientation of foliation planes in the basement gneiss. 'S'-shaped folding of vertically-dipping foliation planes suggests sinistral strike-slip movement. Compass is 6cm wide, and points north. Recorded at 23°06.19'S; 29°00.46'E.

Figure 2.7: An approximately 080°-striking foliation exhibits vertically-plunging folds with asymmetric 'S'-shaped folds, indicative of a sinistral sense of movement. Compass is 6cm wide, and points north. Recorded at 23°05.12'S; 29°01.93'E.

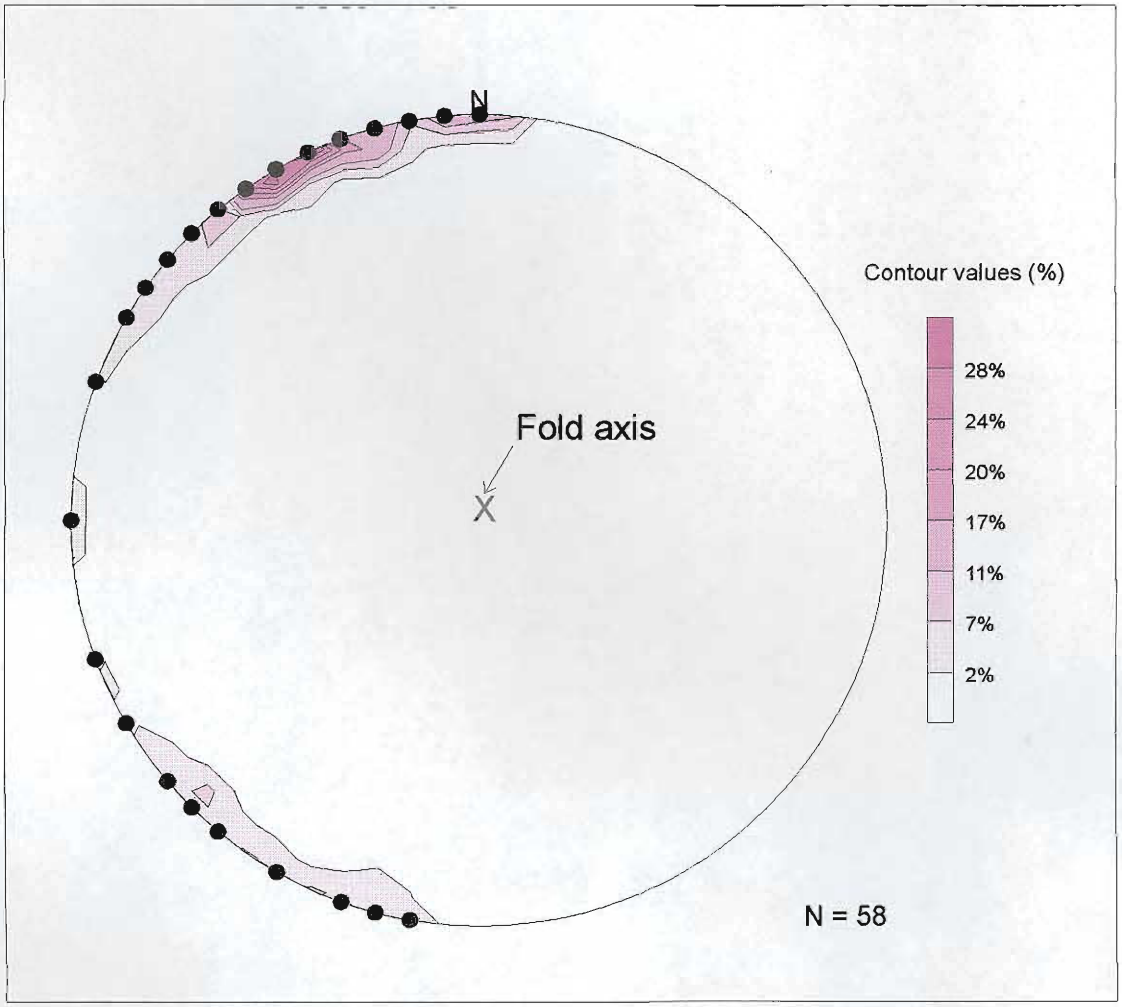

Figure 2.8: Stereographic projection showing poles of foliation planes in 'S' folded basement gneiss.

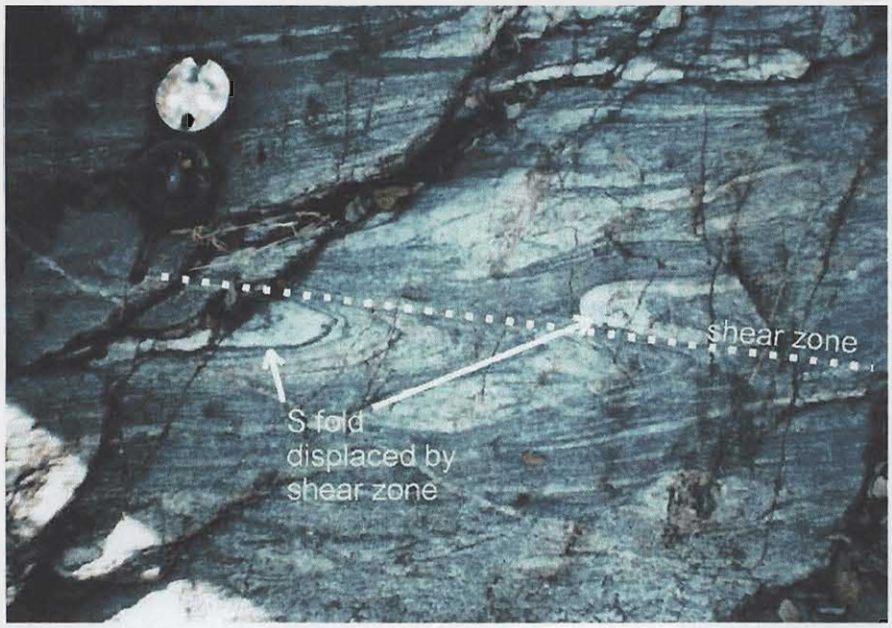

Figure 2.9: A primary foliation, which strikes 042° and shows asymmetric 'S' folds with a vertical plunge is cross-cut by a younger dextral shear zone which strikes 122°. Recorded at 23°05.12'S; 29°01.93'E. Compass is 6cm wide, and points north.

Figure 2.10: Poorly defined foliation in basement gneiss at 23°04.82'S; 28°54.67'E, caused by either partial melting, interferance folding or by injection of melt. Compass is 7 cm wide.

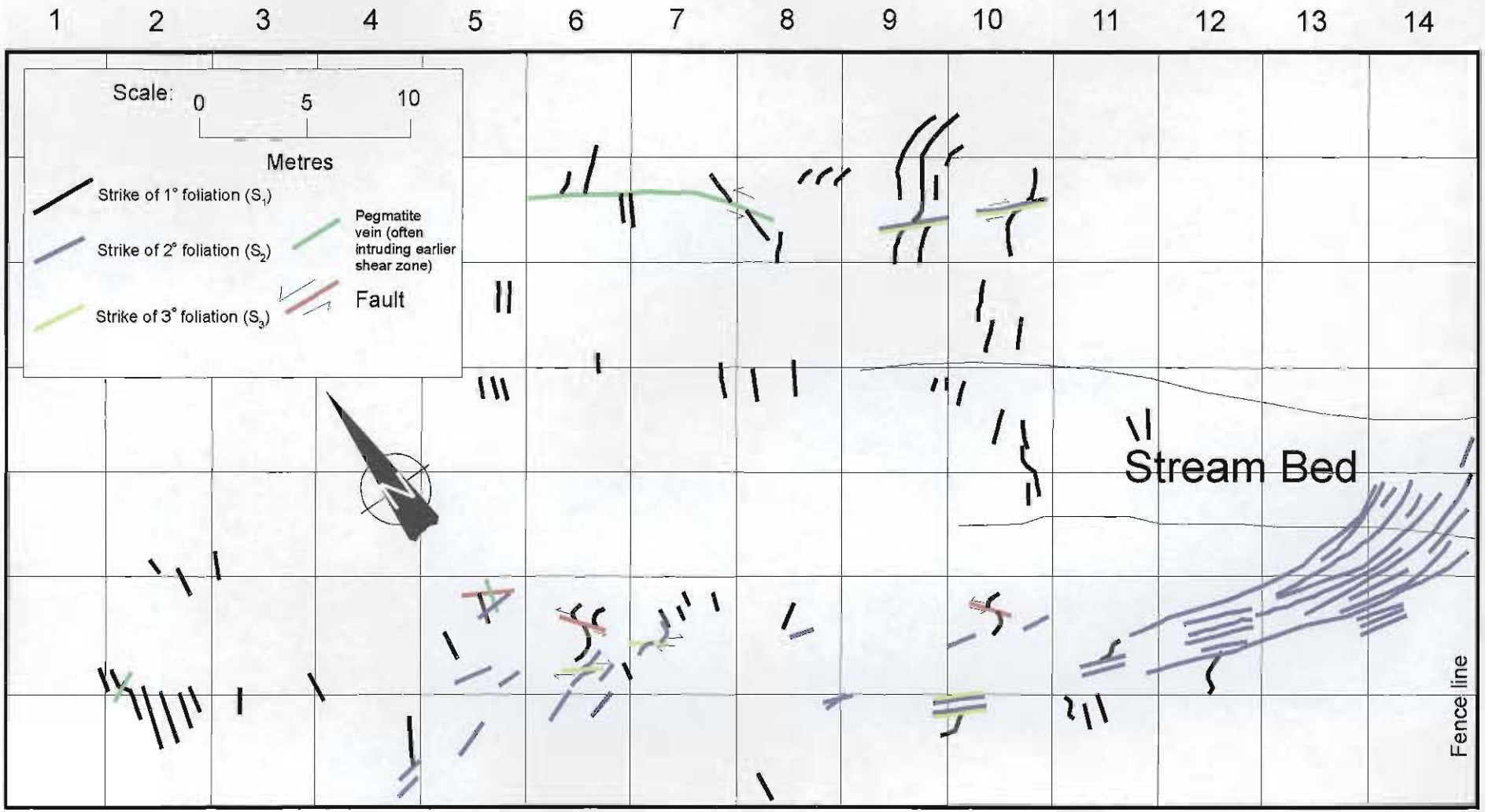

Figure 2.11: Map showing the strike of foliation planes at My Darling (23°05.21'S; 28°47.53'E).

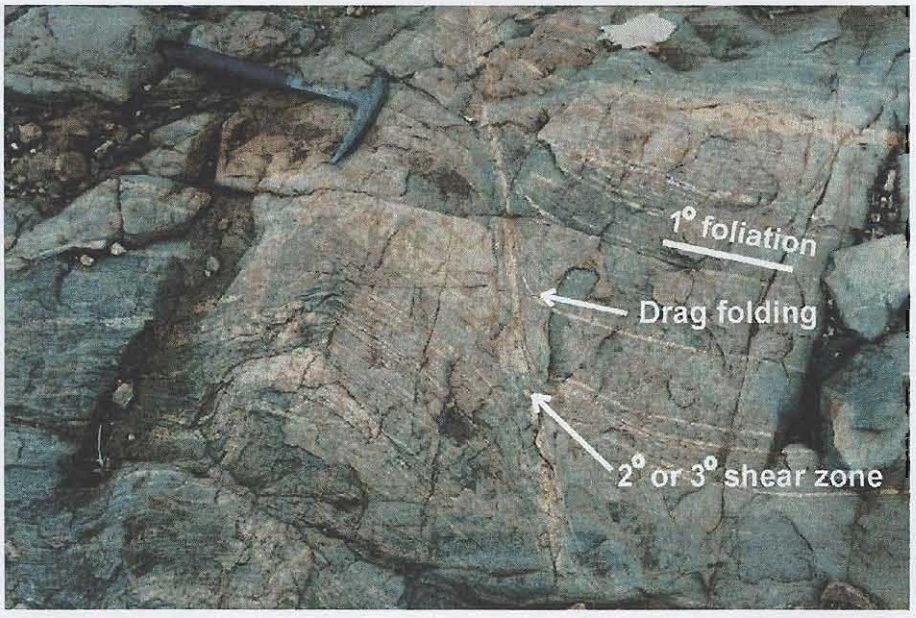

Figure 2.12: Photograph showing detail of grid-square B/10 in Figure 2.11. A primary foliation plane strikes 045°, and is displaced by a secondary or tertiary shear zone, which strikes 115°. Drag folding of the primary foliation suggests that the dextral movement along the later (S_2 or S_3) foliation plane. Hammer is 30cm long.

Figure 2.14: Friable crush breccia from 23°07.39'S; 28°57.46'E, at the southern strand of the Melinda Fault. Lens cap is 5cm wide.

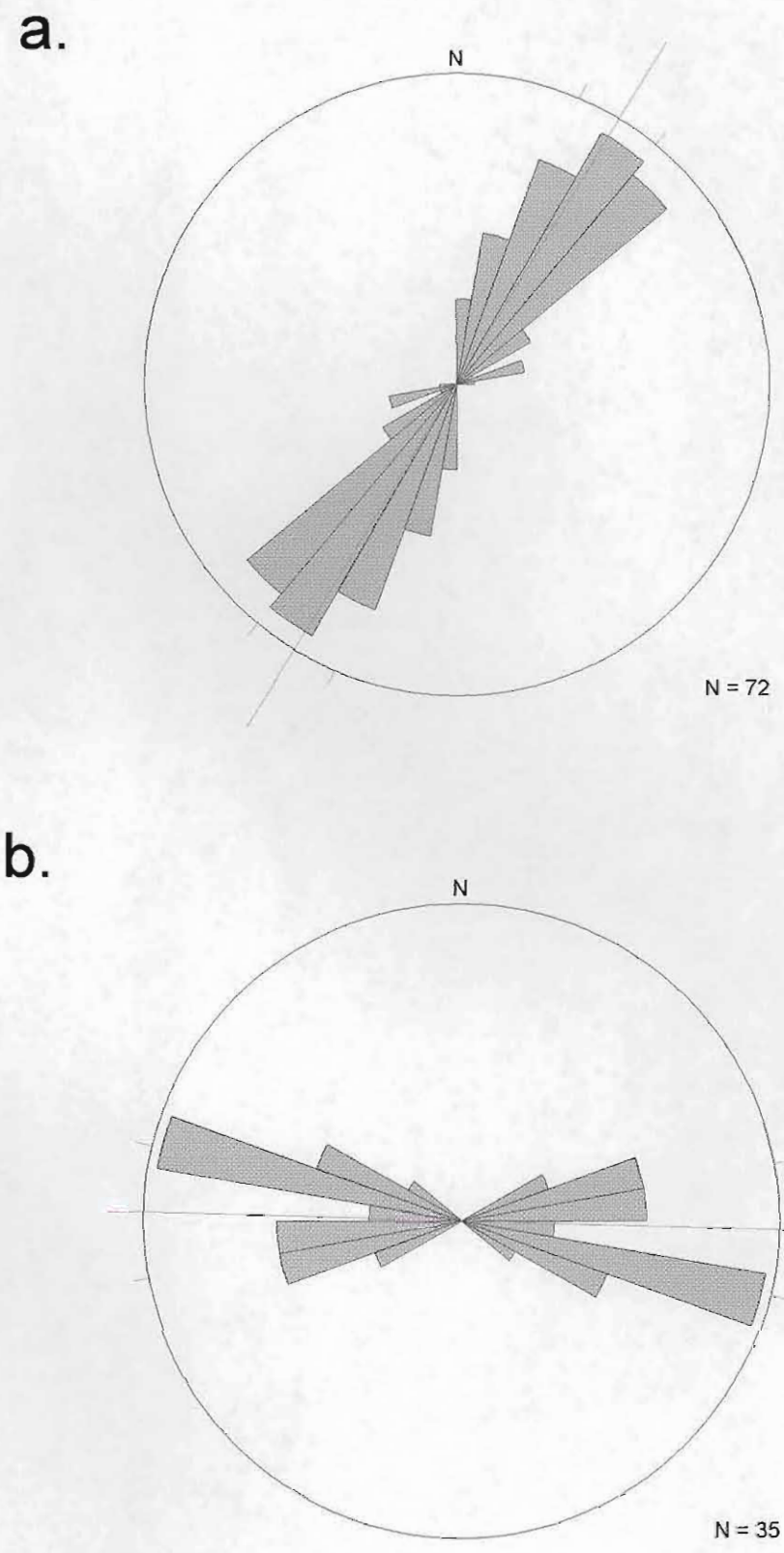

Figure 2.13: Rose histograms showing the strike of (a.) Primary and (b.) Secondary foliation planes in banded gneiss close to My Darling. Principal direction (vector mean) is shown.

Figure 2.15: Crush breccia intruded by thin quartz-filled veins, from 23°07.39'S; 28°57.46'E at the southern strand of the Melinda Fault. Lens cap is 5cm wide.

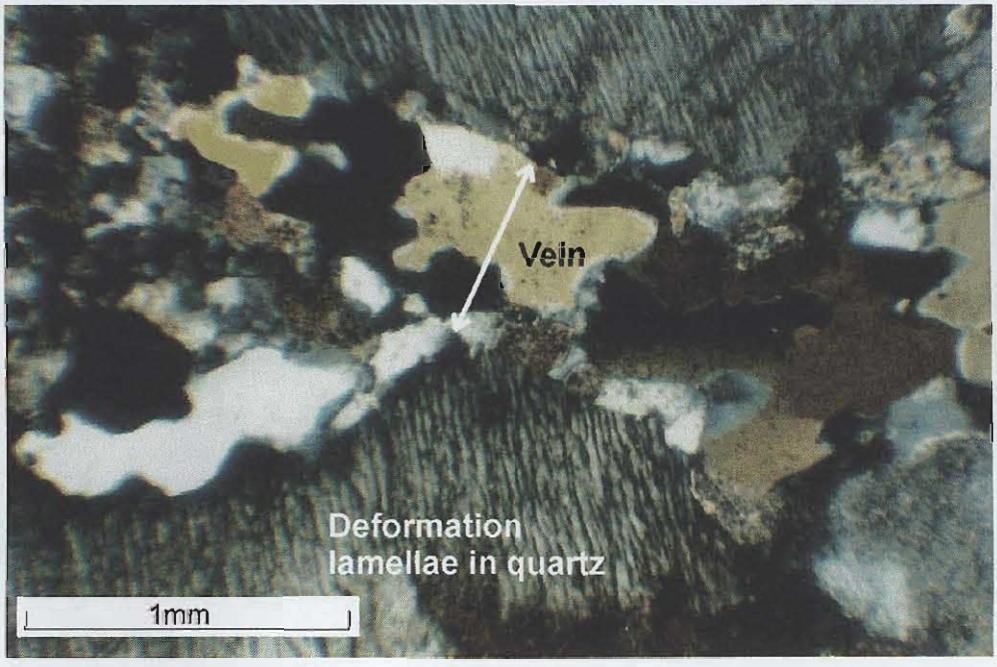

Figure 2.16: Photomicrograph of quarts veins intruding quartzo-feldspathic gneiss at 23°06.31'S; 29°01.16'E. Note that the vein quartz is undeformed compared to deformation lamellae in neighbouring quartz crystals in the gneiss.

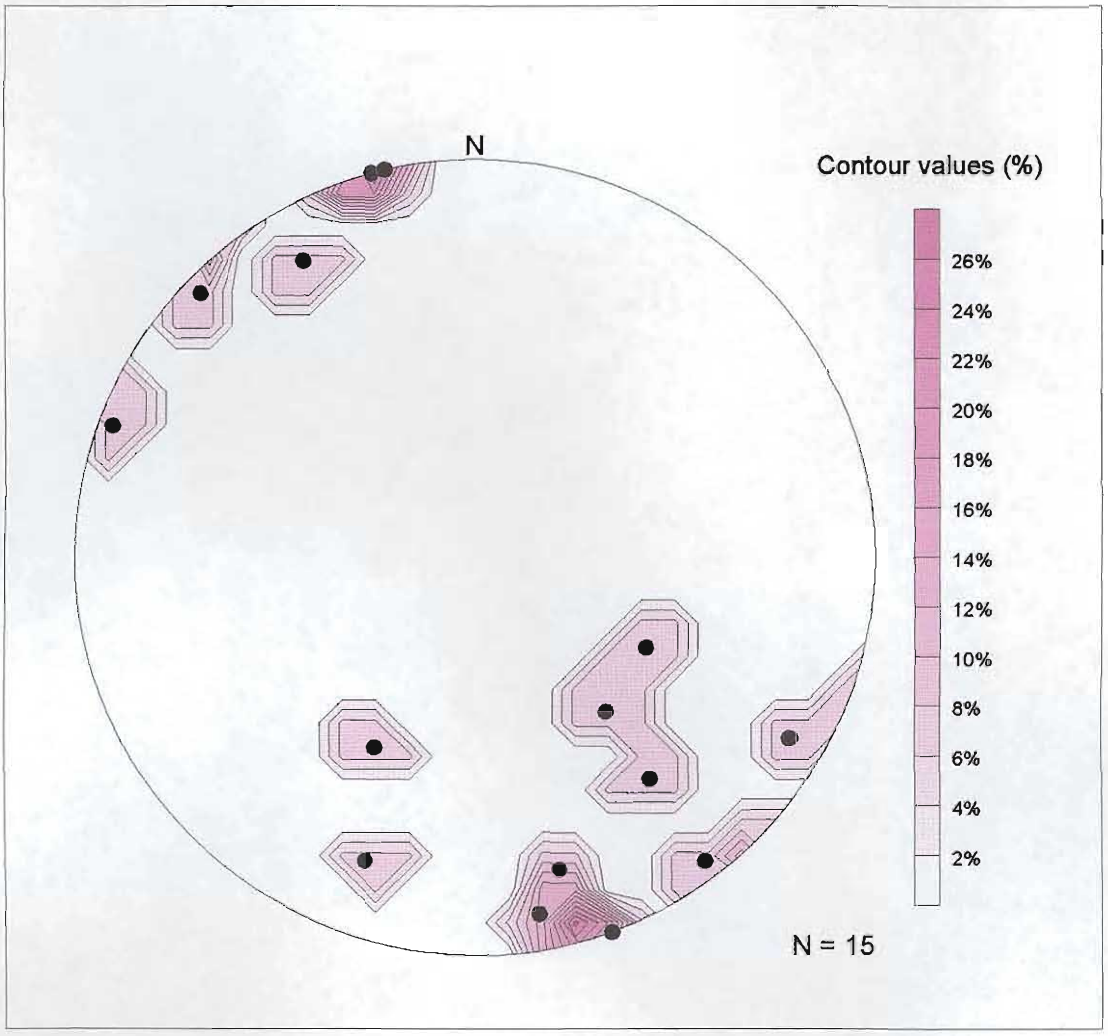

Figure 2.17: Stereographic projection showing the poles to planes defined by quartz-filled veins cutting fault rocks along the southern strand of the Melinda Fault Zone.

Figure 2.18: Hydrothermally altered rock from the contact between the southern strand of the Melinda Fault and the Blouberg Formation at 23°07.39'S; 28°57.46'E. Lens cap is 5cm wide.